PAPER

Modeling and optimization of parameters for high-temperature solid particle erosion of the AISI 446SS using RSM and ANN

Materials Research Express

PAPER

Modeling and optimization of parameters for high-temperature solid particle erosion of the AISI 446SS using RSM and ANN

Ankitendran Mishra[1], **Dhananjay Pradhan**[1], **C K Behera**[1], **S Mohan**[1] and **A Mohan**[2]

[1] Department of Metallurgical Engineering, Indian Institute of Technology (B H U), Varanasi, India
[2] Department of Physics, Indian Institute of Technology (B H U), Varanasi, India

E-mail: ankitendranm.rs.met15@iitbhu.ac.in

RECEIVED
24 August 2018

REVISED
27 September 2018

ACCEPTED FOR PUBLICATION
25 October 2018

PUBLISHED
7 November 2018

Keywords: solid particle erosion, 446 stainless steel, erosion rate, central composite design, regression, artificial neural network

Abstract

In the present study, the effect of high-temperature erosion of AISI 446SS in the temperature range of 350 °C–750 °C using 50 μm alumina particle with the impact angle of 30° − 90° and velocity of 40–100 m s^{-1} is studied using Air Erosion Test Rig, keeping Abrasive flux rate constant at 4.2 gm min^{-1}. Increase in erosion rate (ER) is seen with increasing temperature, which is attributed to change in properties of materials at elevated temperature. A second order polynomial model is developed using response surface methodology (RSM), and effect of the main and interactive parameters on erosion rate is optimized. A well trained artificial neural network (ANN) with back propagation algorithm is used to verify the optimized parameters for erosion rate generated by RSM.

1. Introduction

Impact of a hard solid particle on material surface generates erosive wear, which is commonly seen as a material degradation mechanism in industrial and manufacturing processes. The mechanism of erosion is a complex phenomenon and is greatly affected by several factors. Factors like mechanical properties of the target material, kinetic energy, mass, hardness, the shape of erodent particle and their impact speed and impact angle have been rigorously examined by several researchers in the past to minimize the damage caused by erosion [1, 2]. Shipway *et al* [3] studied the effect of particle and target surface hardness. Smaller size sand particles were found more aggressive in causing the higher degradation to the material. This could be the effect of their difference in inertia force and drag force when compared with larger sized particles [4, 5]. Humphrey [6] suggested that impact parameters are strongly dependent on particles ambient conditions. Oka [7], Finnie [8] and Bitter [9, 10] reported that at low impact angles erosion occurs by cutting action irrespective of particles shape and size. Lopez [11] studied the effect of abrasive velocity and concluded that surface damage increases with increasing impact velocity of the particles.

Amidst these most influencing parameters, the erosion rate of material under high-temperature conditions is not much excavated and thus need more attention. High-temperature erosion wear is a serious problem in coal-burning electricity generation industry which often suffers the direct and indirect loss due to the maintenance of the unit [12]. Gat and Tabakoff [13] found that the erosion damage depends upon the impact angle and the test temperature. Levy *et al* [14] studied the effects of erodent particle size and elevated temperature on the combined erosion-corrosion behavior of a series of Cr-containing steels and found that the morphology of surface oxide was dependent upon the erodent particle size and test temperature, whereas, hardness shows no correlation with erosion rate. The previous investigation has shown that mass loss depends on the material and its testing, and environmental conditions [15]. Environmental factors [16] severely affects the mechanical properties of the materials. Assuming that as the test temperature increases, the hardness and tensile strength of the materials are changed, which may influence the erosion characteristics of the materials. The testing temperature is becoming an important factor in erosive wear since ductile-brittle- transition greatly affects the mass removal mechanism from the surface. When testing temperature increases, plastic deformation and ductile mode of material removal mechanisms like cutting, scratch formation, and craters, are favored [17].

Table 1. Chemical composition of AISI 446SS.

Elements	C	S	P	Si	Mn	Cr	Ni	Mo	N
Wt%	0.068	0.0039	0.021	0.38	0.43	24.07	0.15	0.03	0.1430

In this study, erosion tests were conducted to evaluate the behavior of AISI 446 SS at the higher temperature. These steels, particularly at higher chromium levels, have excellent corrosion resistance, as equal as 18–8 Cr-Ni steels, in many environments. When annealed, are completely free from stress corrosion and are therefore a substitute for the austenitic stainless steel [18]. These steels are suitable for high-temperature applications in heat-exchangers [19]. Dependence of wear rate on temperature was highlighted in Surr's study. The findings illustrated that the wear rate shows no significant change up to 450 °C. Further, in the range between 450 °C to 570 °C a hard protective layer of Fe_2O_3 prevents the erosion. whereas beyond 570 °C a weak film of FeO is formed, which combines with the parent metal and causes a steep rise in the erosion rate [20]. Studying the effect of these variables, there is an enormous scope of implementing statistical techniques for analysis, prediction, and optimization to obtain the maximum benefit. The present investigation addresses this aspect by using Response Surface Methodology (RSM). RSM is a multivariate technique based on the fit of a polynomial equation to a statistical data, with an objective to simultaneously optimize the levels of these variables to attain the best system performance. This technique has been widely used by investigators to optimize different process parameters in several engineering applications [21, 22]. To approximate a response function to experimental data, a quadratic response surface, i.e., Central Composite Rotatable Design (CCRD) is used in the present study.

ANN offers an alternative to the polynomial regression method as a modeling tool. Advances in computing power have enabled the application of ANN in providing non-linear modeling for response surfaces and optimization. McCulloch and Pitts [23] developed an ANN model based on their knowledge of neurology. Paul Werbos [24] contribution of back-propagation learning method is recognized as the most significant contribution. Velten *et al* [25] and Zhang *et al* [26] were among the first to implement ANN to analyze the wear of polymer composites. Palavar *et al* [27] used ANN to predict the wear behavior of IN706 superalloy. To predict the wear behavior of aluminium alloys and its composites, ANN has been widely used [28–30]. More recently work by Suresh *et al* [31] reports successful implementation of ANN in predicting solid particle erosion in composites. A multilayer feed-forward network with back-propagation training algorithm has been used widely in wear prediction [26]. Hence, artificial neural networks (ANNs) have been extensively used for the prediction of wear data in tribological tests [32, 33]. In view of the above, in the present study, the ANN technique has been used for the prediction of high-temperature steady-state erosion rate of AISI 446SS.

2. Experimental

2.1. Materials and methods

AISI 446SS in the form of round bars was used as the test material, and its chemical composition is listed in table 1.

These bars were sectioned into circular disc with 5 mm thickness and 20 mm diameter and mirror polished to a roughness value of ~0.01 μm. Subsequently, test specimens with ASTM G76-95 standard were subjected to erosive wear in a sand blast type erosion tester. The operating parameters, i.e., the temperature in a range of 350 to 750 °C, impact velocity in a range of 40–200 m s^{-1} and impact angle within 30° to 90° were used to study loss in the weight of the samples. Alumina sand with ~50 μm size was used as the erodent. The samples were ultrasonically cleaned using acetone and weighed using the digital balance to an accuracy of 0.01 mg. The erosion rate of the sample has been calculated after 30 min of erosion; however, the samples were weighed at regular interval of 5 min.

$$\text{Erosion Rate(g/g)} = \frac{\text{weight loss of target material}}{\text{weight of the erodent particle impinging on target surface}}$$

The digital photograph of the eroded scar surface is shown in figure 1. It is seen that the appearance on the tested surface differs with test conditions due to the formation of an oxide layer on the surface when exposed to high temperature. These oxides are also considered to act as a protective layer, thereby, prevents the direct contact of abrasives with material surface. Further, worn surfaces were examined using a scanning electron microscope (FEI Nova NanoSEM450) to determine the possible erosion mechanism.

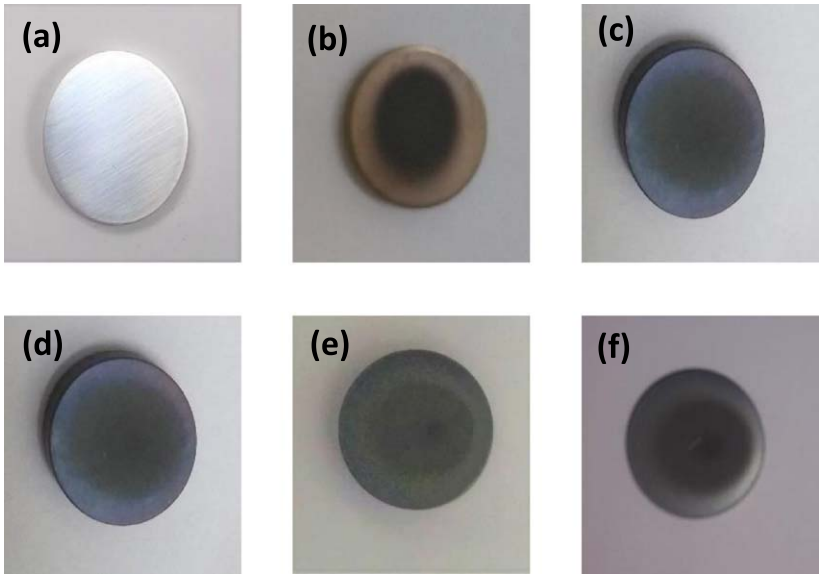

Figure1. Macrograph of (a) un-eroded and (b)–(f) eroded surface under test temperature of 350 °C, 450 °C, 550 °C, 650 °C and 750 °C respectively.

2.2. Response surface methodology (RSM)

RSM is a collection of mathematical and statistical technique that is used for modeling, analysis, and optimization, where the response is influenced by several variables [34]. This is an economical and effective method of optimization which reduces the experiments to a fairly low number. Although RSM employs either linear or square polynomial functions to describe and explore the experimental conditions, second-order models are generally used in RSM as they are flexible and also provide a better approximation to the true response surface [35].

2.3. Artificial neural network (ANN)

ANN is inspired from human brain functions, and consists of highly interconnected processing elements in groups called as neurons. The pattern of interconnecting these neurons is called 'architecture'. The performance of the neural network depends on the number of hidden layers and some neurons in hidden layers, i.e., network structure [36]. Therefore, a computer program 'NEURONET' is developed using PYTHON 3.7 for training the data using three layers, and the result is inferred using the back propagation neural network.

3. Results and discussion

3.1. Central composite rotatable design (CCRD)

CCRD presented by Box and Wilson [37] is most widely preferred for second-order response surface model as they are relatively efficient concerning the number of runs required. Second-order model is usually required to approximate the curvature in the true response surface when the experimenter is close to optimum [34].

The fitted second-order response surface model is given by equation (1):

$$\eta = \beta_o + \sum_{i=1}^{k} \beta_i x_i + \sum_{i=1}^{k} \beta_{ii} x_i^2 + \sum \sum_{i<j=2}^{k} \beta_{ij} x_i x_j \tag{1}$$

Where η is response; x_i (1, 2, … k)is the coded level of k quantitative variables; β_o is the constant term, and $\beta_{i,}$ β_{ii} and β_{ij} are the coefficients of the linear expansion.

Full uniformly rotatable central composite design presents the following characteristics:

(a) Requires an experiment number according to N $= k^2 + 2k + C_{p,}$ where k is the factorial number and (C_p) is the replicate number of the central point.

(b) α- value depends on the number of variables and can be calculated as $\alpha = 2^{(k\text{-}p)/4}$. In the present investigation, its value is 1.682

(c) all factors are studied in five levels ($-\alpha, -1, 0, +1, +\alpha$).

Table 2. Erosion parameters and their levels.

			Levels				
Parameters	Notation	Units	−1.682	−1	0	1	1.682
Test temperature	A	°C	350	450	550	650	750
Impact velocity	B	m/s	40	55	70	85	100
Impact angles	C	Degree	30	45	60	75	90

Table 3. Experimental results for Erosive Wear of AISI 420 SS.

	Erosion parameters			
Experimental run	A	B	C	Erosion rate (gm/gm $\times 10^{-5}$)
1	550	70	60	10.151
2	550	70	60	10.158
3	750	70	60	15.463
4	450	85	45	10.395
5	550	70	30	11.269
6	650	55	75	12.539
7	350	70	60	7.936
8	550	70	60	10.148
9	550	100	60	18.095
10	650	85	75	14.503
11	550	40	60	9.523
12	550	70	90	8.573
13	450	55	45	6.140
14	550	70	60	10.143
15	550	70	60	10.156
16	450	55	75	5.654
17	550	70	60	10.139
18	450	85	75	8.746
19	650	55	45	14.601
20	650	85	45	16.269

Table 4. Analysis of variance for erosion rate.

Source	DF	Adj SS	Adj MS	F-Value	P-Value
Model	9	193.938	21.549	19.25	0.000
Linear	3	170.326	56.775	50.73	0.000
Test temperature	1	115.034	115.034	102.78	0.000
Impact velocity	1	47.223	47.223	42.19	0.000
Impact angles	1	8.068	8.068	7.21	0.023
Square	3	21.435	7.145	6.38	0.011
2-Way Interaction	3	2.177	0.726	0.65	0.602
Error	10	11.192	1.119		
Lack-of-Fit	5	11.192	2.238	41323.96	0.000
Pure Error	5	0.000	0.000		
Total	19	205.130			

Table 2 presents the process parameters at five different levels, and table 3 shows the design matrix of twenty iterations, according to CCRD technique, to calculate the erosion rate of the sample. To analyze the regression model, a software package of MINITAB 18 has been used.

3.2. Analysis of variance and regression model for Erosion rate

The regression coefficients evaluated using ANOVA has significantly determined each factor regarding erosion rate as shown in table 4. The model for erosion rate employing $R^2 = 94.54\%$ signifies that the model is compatible with total variance at 95% confidence limit. P-values less than 0.05 reveal that the model is statically significant for optimization.

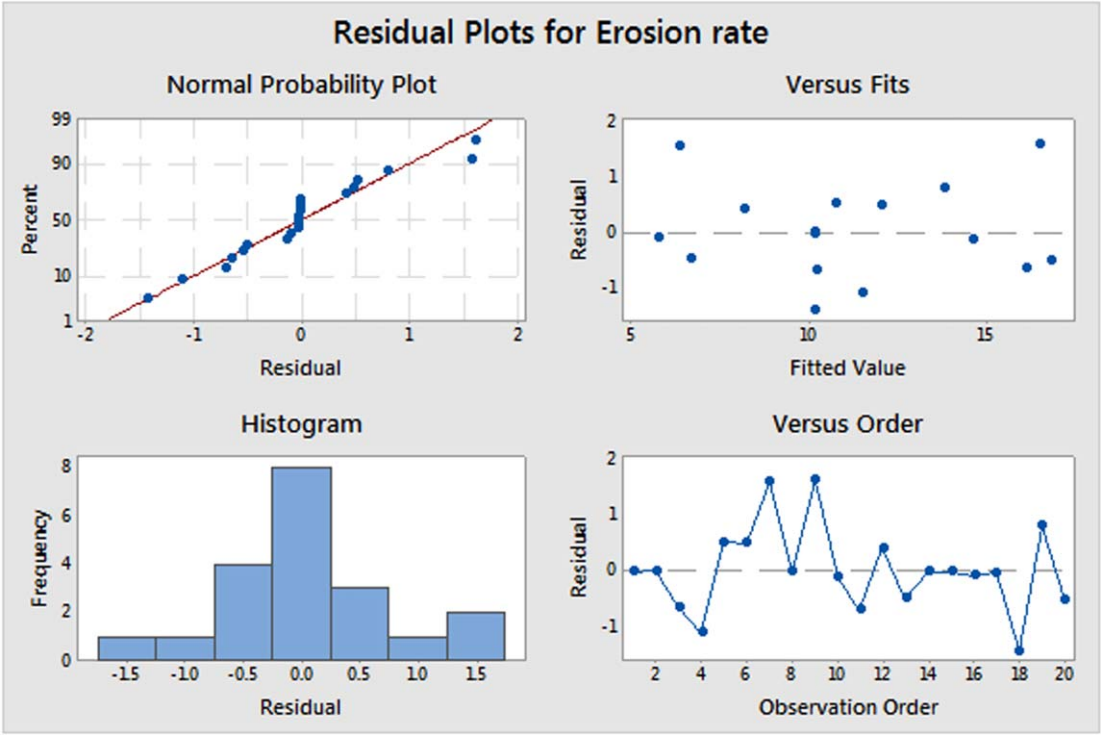

Figure 2. Residual normal probability plots for erosion rate.

Response surface regression equation is obtained as:

$$\text{Erosion rate} = 10.175 + 2.902\,\text{A} + 1.860\,\text{B} - 0.769\,\text{C} + 0.378\,\text{A*A} + 1.224\,\text{B*B} - 0.250\,\text{C*C} - 0.464\,\text{A*B} - 0.212\,\text{A*C} - 0.108\,\text{B*C}$$

$$R^2 = 94.54\%$$

Normal probability plot shown in figure 2 confirms that all the residues are falling on a straight line with errors being positioned normally and no scattering is observed. Percentage contribution of each parameter measures tests temperature as the most influencing parameter with 56.07%.

Figure 3 shows the 3D- and 2D- surface contour plots of variation in erosion rate with the input parameter. It is observed from the contours that increase in impact velocity, impact angle and test temperature plays a vital role. With increase in input parameters, the material removal mechanisms like cutting and plastic deformation are more intense. Therefore, ER is seen to increase with increase in input parameters. Figure 4 shows the SEM micrograph of the worn surface which substantiates the above statement. This micrograph shows that, keeping one parameter constant, increase in two input variables increases width and depth of cut. Thereby, plastically deforming of the materials is in the form of lips. Similar behavior was reported in our earlier publication [38].

The average surface roughness of the worn surface (figure 4) was analyzed using Atomic Force Microscope (AFM). The results obtained are shown in figure 5 and the values are tabulated in table 5. Here, a rougher surface with more irregularities in topography is observed as stainless steel AISI 446SS was eroded using higher values of 'test temperature—impact velocity', shown in figure 3(a). Also, on selecting 'impact velocity—impact angle', (figure 3(b)) it is observed that mild erosion rate occurs with lower values of input parameters. With further increase in impact velocity, erosion rate significantly increases for a moderate increase in impact angles. Whereas, reduction in erosion rate is recorded for higher values of both the input parameters. This indicates the occurrence of steady state of erosive wear. This may be due to formation of work-hardened subsurface under the impact area.

Considering the input parameters 'test temperature- impact angle', the erosion rate is seen to increase with higher values of input parameters. However, beyond a certain level, with further increase in impact angle, the erosion rate is reduced to a moderate value. This is due to the smeared surface created over a larger area during low angle impact. Still, the test temperature effect is more prevalent. Main effect plot for erosion rate with test temperature, impact velocity, and impact angle is shown in figure 6.

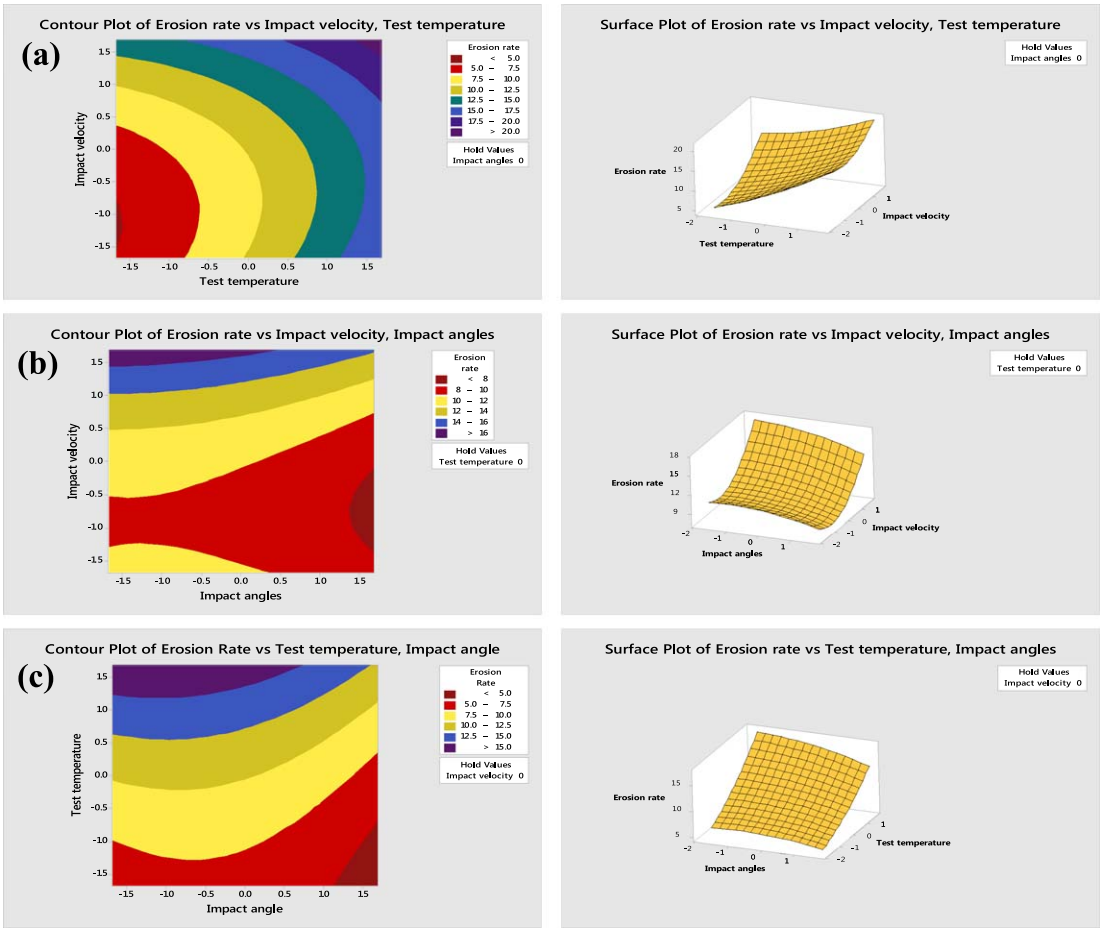

Figure 3. 2D-contour and 3D- surface plot showing Erosion rate variation with (a) test temperature—impact velocity (b) impact velocity-impact angle (c) test temperature- impact angle.

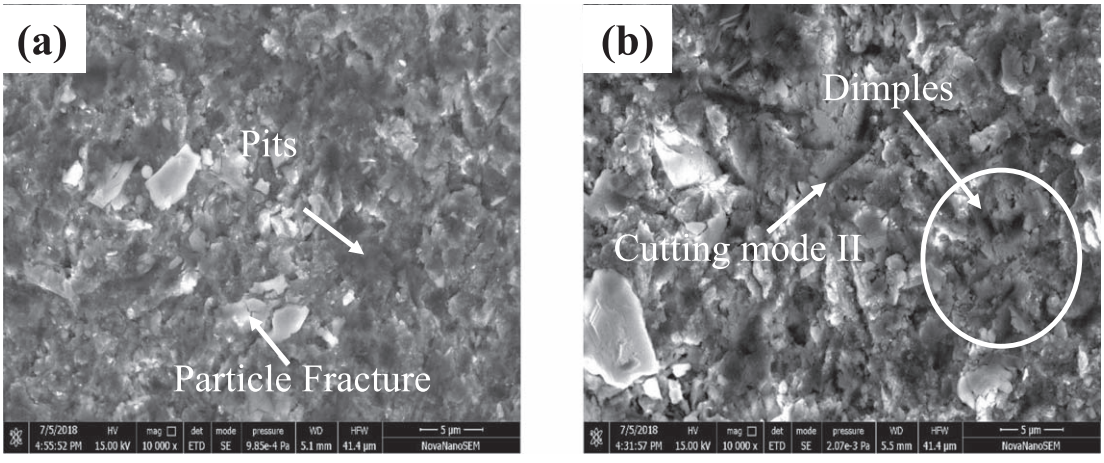

Figure 4. SEM macrograph of tested sample at (a) 450 °C, 55 m s^{-1},45° and (b) 650 °C, 85 m s^{-1}, 45°.

3.3. Prediction using artificial neural network

The database is divided into three categories, namely: (i) a validation category (ii) a training category (iii) a test Category. In the training phase, each neuron receives the input signals xi from n neurons, assign the weights (Wij) of the synapses to each of these inputs, according to equation (2), and passes the result as the output signal Yi, after applying the sigmoid function, equation (3), as the transfer function.

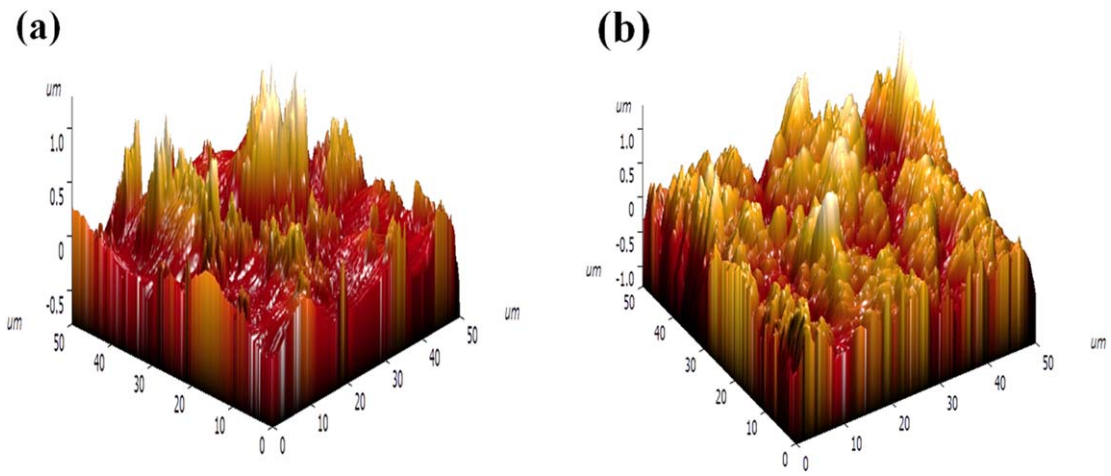

Figure 5 Average Roughness (R_a) values at (a) 450 °C, 55 m s^{-1}, 45° (b) 650 °C, 85 m s^{-1}, 45°.

Table 5. Surface roughness of un-eroded and eroded surfaces.

		Eroded surfaces	
Surface roughness	Un-eroded	450 °C, 55 m s^{-1}, 45°	650 °C, 85 m s^{-1}, 45°
Ra(μm)	0.0104	0.158	0.224

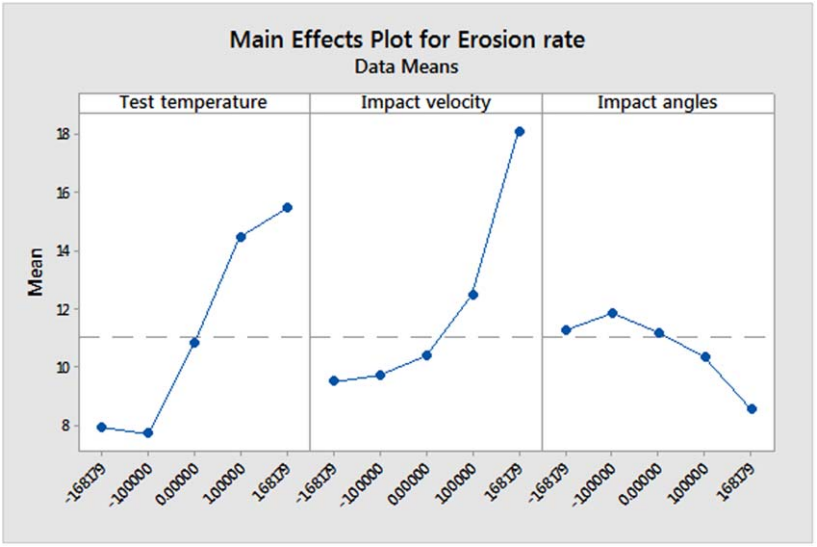

Figure 6. Main effects plot for erosion rate with test temperature, impact angle and impact velocity.

$$Y_i = \sum_{i=1}^{n} x_i w_{ij} \tag{2}$$

$$f = \frac{1}{1 + e^{-x}} \tag{3}$$

The error is minimized by adjustments of the weights according to the following mathematical equation (4);

$$\Delta W_{ij} = \eta \frac{\partial E}{\partial W_{ij}} \tag{4}$$

where η is learning rate parameter.

Table 6. ANN training parameters.

Input parameters for training	Values
Learning parameter (η)	0.001
No. of iterations	1000000
No. of layers	3
No. of neurons in input layer	3
No. of neurons in hidden layer	5
No. of neurons in output layer	1

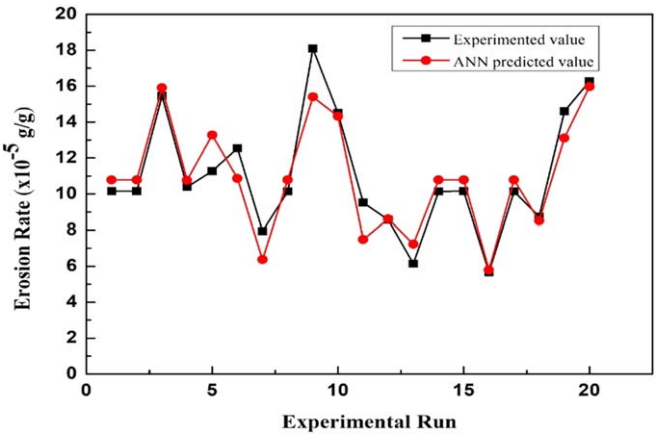

Figure 7. Erosion rate comparison between ANN predicted values and experimented values.

The training parameters for the present study are listed in table 6. A well trained ANN can be used to predict new results in the same knowledge domain. During the evaluation 20 data sets have been used to train the network and optimized parameters for minimum erosion obtained through RSM have been used to test the network. Figure 7 shows the prediction quality of ANN structures based on mean square error.

Table 7 shows that error for experimented sets lies in the range of ~21%. And the error for the optimized parameter is 9.12%, as shown in table 8, which establishes the validity of neural computation.

3.4. Optimization and validation of the model

The aim of validating the model is fulfilled by comparing the predicted results of the model with experimental results. The optimized conditions are listed in figure 8, considering the outline erosion process to be minimized, and values for predicted and experimented results of erosion rate are tabulated in tables 8 and 9 respectively. RSM has been used to get maximum amount of information in a short period of time and with least number of experiments. To investigate the effect of temperature-velocity-angle, for a constant discharge, 3D response surface is plotted. These plots are useful in analyzing interaction between parameters and to obtain their optimum condition for minimizing erosion rate. Effect of input parameters as well as maximum and minimum points for erosion are shown in figures 3(a)–(c). The interaction between input parameters at low temperature, moderate velocity and high impact angle are the most optimized parameters for minimizing loss of materials.

The ANN used focuses on establishing of relationship between input and output parameters. Its evaluation capabilities are based on comparison of predicted capabilities versus the real ones. It was important to test the neural model abilities to generalize and predict synergistic effect of input parameters on erosion behavior of material. Based on neural network analysis ANN showed quite good performance in predicting the erosion rate. This network was used to work with DOE and RSM to optimize erosion rate. The optimization is performed using Minitab Response Optimizer, and the optimum parameters that resulted in minimum erosion rate: test temperature of 350 °C, impact velocity of 55 m s^{-1} and impact angle of 90°. It is observed that as the test temperature and impact velocity increases, the erosion rate also increases. However, with increase in impact angle, erosion rate decreases. The materials exhibits ductile behavior, therefore, results in reduced erosion at normal impact. Three confirmatory tests are performed to check the adequacy of the predicted model with the experimented model. It is inferred that the error lies between 7.54% and 12.81%. This error is due to process incapability since machine follows a normal distribution and therefore, replication of any experimented results follows deviation. The error is assessed as small, and therefore the model is satisfactory.

Table 7. Comparison of experimental and neural network output for test data set.

	Input (Erosion Parameters)			Output (Erosion Rate $\times 10^{-5}$ g g^{-1})		
Experimental run	Test temperature	Impact velocity	Impact angle	Experimental	ANN	Error %
1	550	70	60	10.151	10.787	6.26
2	550	70	60	10.158	10.787	6.19
3	750	70	60	15.463	15.911	2.90
4	450	85	45	10.395	10.763	3.54
5	550	70	30	11.269	13.285	17.90
6	650	55	75	12.539	10.869	−13.31
7	350	70	60	7.936	6.3646	−19.81
8	550	70	60	10.148	10.787	6.29
9	550	100	60	18.095	15.407	−18.80
10	650	85	75	14.503	14.3295	−1.19
11	550	40	60	9.523	7.481	−21.44
12	550	70	90	8.573	8.623	0.58
13	450	55	45	6.140	7.2216	17.61
14	550	70	60	10.143	10.787	6.34
15	550	70	60	10.156	10.787	6.21
16	450	55	75	5.654	5.792	2.44
17	550	70	60	10.139	10.787	6.39
18	450	85	75	8.746	8.504	−2.76
19	650	55	45	14.601	13.118	−10.15
20	650	85	45	16.269	15.974	−1.81

Table 8. Predicted values of the model for erosion rate.

		Erosion rate (g/g $\times 10^{-5}$)	
Parameters	Optimum values	CCRD values	ANN values
Test temperature	350 °C		
Impact velocity	55 m s^{-1}	3.618	3.948
Impact angles	90°		

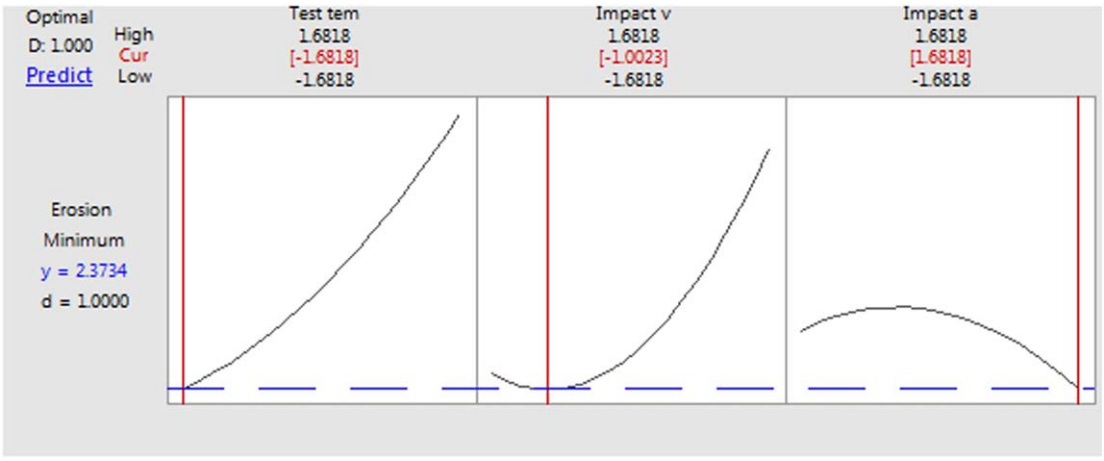

Figure 8. Optimum results for minimum erosion rate.

4. Conclusions

To avoid redundancy in a number of experiments and time consumption, optimization of erosion rate with variable input parameters is essential. Following are the conclusions drawn from the present study:

Table 9. Experimented values for erosion rate.

Test No.	Optimum values	Erosion rate (g/g $\times 10^{-5}$)	Error (%)
1	350 °C	4.081	12.81
2	55 m s^{-1}	3.891	7.54
3	90°	3.997	10.45

1. The results reveal that 'test temperature' is the most dominant factor for erosion rate followed by impact velocity and impact angle.
2. The mathematical model helps in achieving the optimum parameters, of 350 °C test temperature, 55 m s^{-1} impact velocity, and 90° impact angle, to achieve minimum erosion rate.
3. Conformity tests with error value between 7.54% and 12.81% indicated that the model equation is in good agreement with experimental values.
4. The results are in accordance with the established theory of maximum wear rate with oblique impact and vice-versa.
5. Artificial neural network technique was applied to predict the erosion rate of AISI 446SS. The error of 9.12% in the result shows the acceptability of predicted data when compared to measured values.

ORCID iDs

Ankitendran Mishra https://orcid.org/0000-0001-8326-4906
Dhananjay Pradhan https://orcid.org/0000-0002-5511-7826

References

[1] Lin N, Arabnejad H, Shirazi S A, McLaury B S and Lan H 2018 Experimental study of particle size, shape and particle flow rate on Erosion of stainless steel *Powder Technol.* **336** 70–9
[2] Shimizu K and Noguchi T 1994 Erosion characteristics of ductile iron with various matrix structures *Wear* **176** 255–60
[3] Shipway P H and Hutchings I M 1996 The role of particle properties in the erosion of brittle materials *Wear* **193** 105–13
[4] Laitone J A 1979 Aerodynamic effects in the erosion process *Wear* **56** 239–46
[5] McI H 1992 Clark, The influence of the flow field in slurry erosion *Wear* **152** 223–40
[6] Humphrey J A C 1990 Fundamentals of fluid motion in erosion by solid particle impact *Int. J. Heat Fluid Flow* **11** 170–95
[7] Oka Y I, Ohnogi H, Hosokawa T and Matsumura M 1997 The impact angle dependence of erosion damage caused by solid particle impact *Wear* **203** 573–9
[8] Finnie I 1958 *The Mechanism of Erosion of Ductile Metals* (US National Congress of Applied Mechanics)
[9] Bitter J G A 1963 A study of erosion phenomena part I *Wear* **6** 5–21
[10] Bitter J G A 1963 A study of erosion phenomena part II *Wear* **6** 169–90
[11] Lopez D A, Congote J P, Cano J R, Toro A and Tschiptschin A P 2005 Effect of particle velocity and impact angle on the corrosion–erosion of AISI 304 and AISI420 stainless steels *Wear* **259** 118–24
[12] Stringer J 1995 Practical experience with wastage at elevated temperature in coal combustion system *Wear* **186** 11–27
[13] Gat N and Tabakoff W 1978 Some effects of temperature on the erosion of metals *Wear* **50** 85–94
[14] Levy A V, Yan J and Patterson J 1986 Elevated temperature erosion of steels *Wear* **108** 43–60
[15] Abbade N P and Crnkovic S J 2000 Sand–water slurry erosion of API 5L X65 pipe steel as quenched from intercritical temperature *Tribol. Int.* **33** 811–6
[16] Shimizu K, Naruse T, Xinba Y, Kimura K, Minami K and Matsumoto H 2009 Erosive wear properties of high V–Cr–Ni stainless spheroidal carbides cast iron at high temperature *Wear* **267** 104–9
[17] Aiming F, Jinming L and Ziyun T 1996 An investigation of the corrosive wear of stainless steels in aqueous slurries *Wear* **193** 73–7
[18] Bhadeshia H and Honeycombe R 2006 *Steels: Microstructure and Properties* (Oxford: Butterworth-Heinemann) pp 276–7
[19] Guimaraes A A and Mei P R 2004 Precipitation of carbides and sigma phase in AISI type 446 stainless steel under working conditions *J. Mater. Process. Technol. 155-* **156** 1681–9
[20] Ilmar K and Kulu P 2008 *Solid Particle Erosion : Occurance Prediction and Control* (Berlin: Springer) pp 37–40
[21] Chang B P, Akil H M, Nasir R B and Khan A 2015 Optimization on wear performance of UHMWPE composites using response surface methodology *Tribol. Int.* **88** 252–62
[22] Lin J F and Chou C C 2002 The response surface method and the analysis of mild oxidational wear *Tribol. Int.* **35** 771–85
[23] McCulloch W S and Pitts W 1943 A logical calculus of the ideas immanent in nervous activity *The bulletin of mathematical biophysics* **5** 115–33
[24] Werbos P J 1988 Backpropagation: past and future In:*Proc. of the Second Int. Conf. on NeuralNetwork (Piscataway, NJ)* (IEEE) (1) pp 343–53
[25] Velten K, Reinicke R and Friedrich K 2000 Wear volume prediction with artificial neural networks *Tribol. Int.* **33** 731–6
[26] Zhang Z, Barkoula N M, Karger - Kocsis J and Friedrich K 2003 Artificial neural network predictions on erosive wear of polymers *Wear* **255** 708–13

[27] Palavar O, Ozyurek D and Kalyon A 2015 Artificial neural network prediction of aging effects on the wear behavior of IN706 superalloy *Mater. Des.* **82** 164–72
[28] Ozyurek D, Kalyon A, Yıldırım M, Tuncay T and Çiftçi I 2014 Experimental investigation and prediction of wear properties of Al/SiC metal matrix composites produced by thixomoulding method using artificial neural networks *Mater. Des.* **63** 270–7
[29] Kumar S A, Raman S G S, Narayanan T S and Gnanamoorthy R 2013 Prediction of fretting wear behavior of surface mechanical attrition treated Ti–6Al–4V using artificial neural network *Mater. Des.* **49** 992–9
[30] Durmuş H K, Ozkaya E and Meri C 2006 The use of neural networks for the prediction of wear loss and surface roughness of AA 6351 aluminium alloy *Mater. Des.* **27** 56–159
[31] Suresh A, Harsha A P and Ghosh M K 2009 Solid particle erosion studies on polyphenylene sulfide composites and prediction on erosion data using artificial neural networks *Wear* **266** 184–93
[32] Harsha A P and Nagesh D S 2007 Prediction of weight loss of various polyaryletherketones and their composites in three-body abrasive wear situation using artificial neural networks *J. Reinf. Plast. Comp.* **26** 1367–77
[33] Jiang Z, Gyurova L, Zhang Z, Friedrich K and Schlarb A K 2008 Neural network based prediction on mechanical and wear properties of short fibers reinforced polyamide composites *Mater. Des.* **29** 628–37
[34] Montgomery D C 2001 *Design and Analysis of Experiments* (New York: Wiley,)
[35] Palanivel R, Mathews K and Murugan N P 2013 Optimization of process parameters to maximize ultimate tensile strength of friction stir welded dissimilar aluminium alloys using response surface methodology *J. Cent. South Univ.* **20** 2929–38
[36] Rajasekaran S and Pai G V 2003 *Neural Networks, Fuzzy Logic and Genetic Algorithm: Synthesis and Applications* (New Delhi: PHI Learning Pvt. Ltd)
[37] Box G E P and Hunter J S 1957 Multi-factor experimental designs for exploring response surfaces *The Annals of Mathematical Statistics* **28** 195–241
[38] Mishra A, Behera C K, Mohan S and Mohan A 2018 Erosive Wear of 446SS Ferritic Steel: A Potential Material for Heat Exchangers Application *Mater. Res. Express* **5** 106522